Surface Microprocessing AISI-O1 by Pulsed Nd: YAG Laser

Kelvii Wei Guo[*]

Department of Mechanical and Biomedical Engineering, City University of Hong Kong, 83 Tat Chee Avenue, Kowloon Tong, Kowloon, Hong Kong

Abstract: Due to tedious and time-consuming work put into the conventional mold/die microprocessing (about 37% of the total time of the entire mold/die production). Therefore, to improve or enhance the quality of mold/dies at the final step with a less number of trained and skilled operators or decrease the processing time to cut the overall cost dramatically, AISI-O1 cold work steel was micro-processed by Pulsed Nd: YAG laser. The influence of laser processing parameters on the evolution of the correlated surface morphology was investigated by a 3D profilometer, scanning electron microscopy (SEM), and optical microscopy (OM). The results show that when AISI-O1 specimens were irradiated with various parameters, the morphology of AISI-O1 cold work steel was changed correspondingly. It also demonstrates that the different kinds of micro-processed surface morphology could be established successfully to satisfy the later practical requirements for a given laser. Meanwhile, the effect of laser processing parameters on the relevant temperature was described, and the laser microprocessing temperature field was also proposed. It reveals that the influence of laser pulse feed rate was more prominent than that of other parameters on the relevant micro-processed surface morphology.

1. INTRODUCTION

The quality requirements of dies and molds are high for the fabrication of glass, metal, and plastic products. Small abrasive tools or wheels that can rotary and vibrate by themselves can enhance the easily accessible areas of some surfaces. However, in the practical situation, the surface of these dies and molds is mainly finished or processed by hand. The processing has mainly relied on the successive size decrement of particles taken for abrasion distributed on abrasive papers or cloths in order to make the finished surface meet with practical applications.

The shortcomings of operators create many limitations during manual processing. It should be noted that operators have to be seriously trained to gain considerable experience and meet the requirements of practical operations under various conditions, especially with the small radii equipment, to attain effective application. Moreover, it also requires a consistent and repeatable operation. In addition, it requires a skilled operator to take ten days to process ten dies with complicated forms. Meanwhile, it also needs to make sure that all the finished dies are identical after completion. More importantly, the accuracy of the die dimension is not lost after

the finished surface is achieved. Therefore, an operator with high experience and skills is definitely expensive. It is well known that a well-trained operator is essential to the process of manufacturing.

As mentioned above, it can be seen that it is extremely tedious and time-consuming for this process. The research shows that the time consumed on mold finishing can be about 37% of the total time of the entire mold production [1]. Therefore, it is crucial and urgent to improve or enhance the quality of the die or mold at the final step with fewer trained and skilled operators or a decrement in processing time to cut the overall cost dramatically.

There are also some limitations to the closed dies processing for the processes with automatic techniques. The investigation shows that it is very slow for precision machining by a single-point diamond tool. Moreover, it is not readily available in industrial conditions and is hard for flat surfaces [1-3]. Chemical and electrochemical micromachining are limited in their applications and can be difficult to control [3-6]. Moreover, the relevant chemical approaches are undesirable due to the use of un-ecofriendly chemicals and difficulties in the selective removal of material. Some research has been carried out into the use of robot-controlled finishing tools [1-3, 5-9]. However, using a rotary wheel or ultrasonic chisel requires that the being micromachined surface be almost parallel to the wheel's axis or the chisel

*Department of Mechanical and Biomedical Engineering, City University of Hong Kong, 83 Tat Chee Avenue, Kowloon Tong, Kowloon, Hong Kong; E-mail: kelviiguo@yahoo.com

Table 1: **Chemical Composition of AISI-O1 Cold Work Steel**

Element	C	Si	Mn	Cr	W	V	Fe
(wt.%)	0.9	0.3	1.2	0.5	0.5	0.1	Bal.
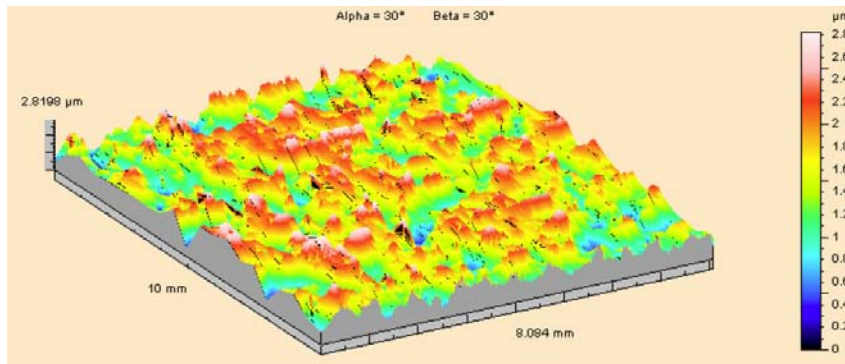
Figure 1: Initial morphology of specimen Ra= 0.4 μm.

angle. As a result, it is not suitable for almost flat workpieces and limits its applications.

Ultrasonic machining can be used to remove the controllable material [1, 3]. By this technique, the hammering force between the abrasive particles (in the water-based slurry) and the workpiece at high frequency can remove the material from the processed surface. So, shapes with complicated forms can be achieved with suitably designed tools. Although it is the potential for processing closed molds or dies, there are still some disadvantages, especially for the indentation of workpieces and the drilling of the fixed location.

Currently, it is efficient and successful to apply abrasive flow machining to process the open molds or dies. In this process, a mix of abrasive particles is taken to finish the surface by hydraulic power in the form of a suspension in a pliable polymer base. However, the limitation is still to restrict this process from finishing the molds or dies without an exit and an entry for the flowing mix in the hollow or tubular form [1, 2].

Now, the laser is widely used as a machine tool to modify the surface of engineering materials, such as laser surface alloying, laser cladding, surface texturing, laser physical vapor deposition, *etc*. [1, 7-12]. In recent years, laser microprocessing is becoming an attractive new technique for machine lenses, diamonds, *etc*. [13-20].

By considering the unique characteristics of the laser radiation and its excellent non-contact microprocessing possibility, an investigation has been made to process AISI-O1 steel employing the concepts of microprocessing.

2. EXPERIMENTAL MATERIAL AND PROCEDURES

2.1. Experimental Material

The chemical composition of AISI-O1 cold work steel is shown in Table **1**.

2.2. Experimental Procedures

The materials were cut into 25 mm'10 mm'10 mm and carefully cleaned with acetone and pure ethyl alcohol to remove any contaminants on their surface. Figure **1** shows the Talysurf 3D morphology of the original AISI-O1 specimens with the initially machined surface roughness Ra=0.4 μm, whilst Figure **2** shows the corresponding 2D SEM morphology.
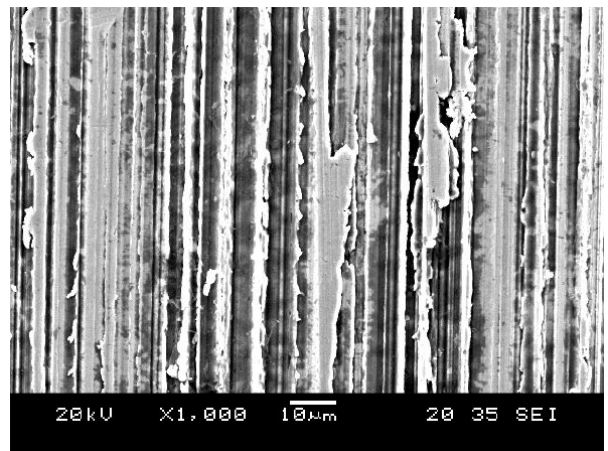
Figure 2: SEM result of AISI-O1 initial surface.

A GSI Lumonics Model JK702H pulsed Nd: YAG TEM_{00} mode laser system, with a wavelength of 1.06 μm, a defocused distance of 15 mm, and a focus spot diameter of approximately 1.26 mm on the substrate surface, was used to irradiate AISI-O1 steel.

The different laser microprocessing conditions employed were as follows:

Laser feedrate/Scanning speed: 100, 200, 300, 400 mm/min.

Pulse energy (P): 1, 2, 3 J.

(a) 100 mm/min

(b) 200 mm/min

(c) 300 mm/min

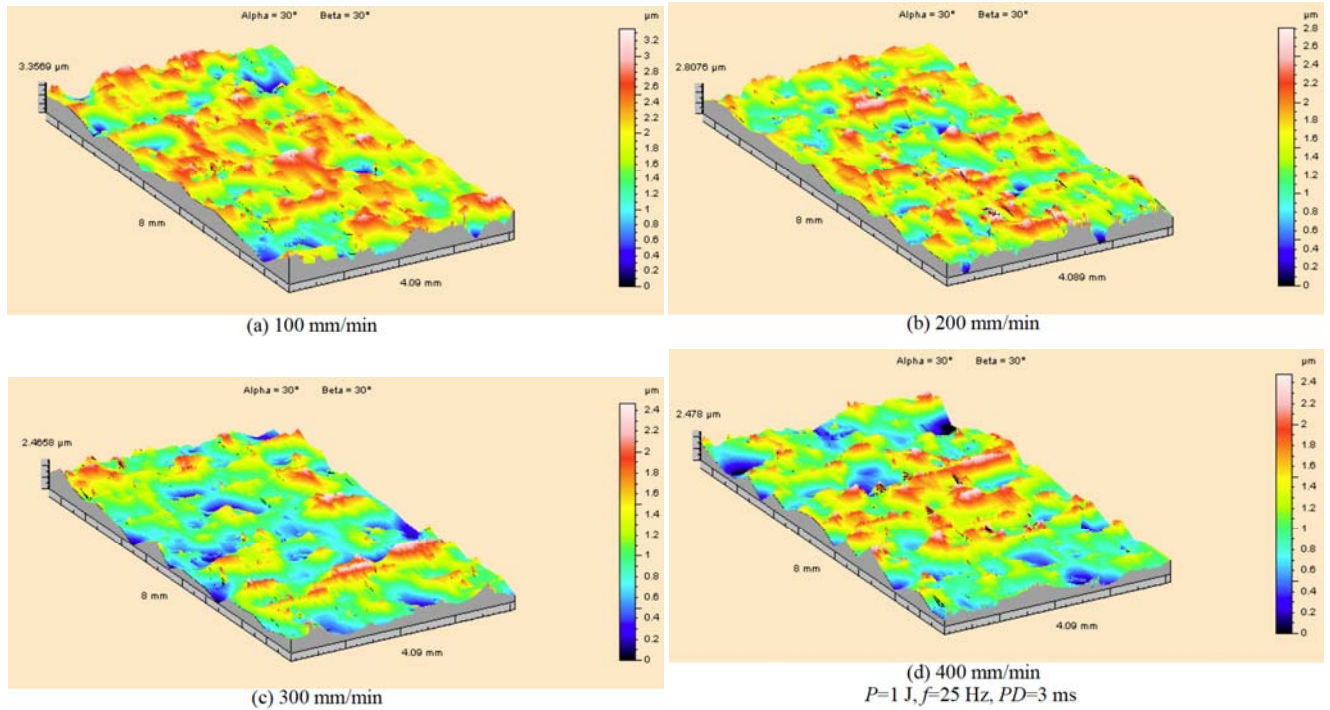(d) 400 mm/min
$P=1$ J, $f=25$ Hz, $PD=3$ ms

Figure 3: Surface morphology of laser microprocessing AISI-O1 steel at various feed rates.

Pulse duration (*PD*): 2, 3, 4, 5, 6 ms.

Pulse frequency/ Repetition rate (*f*): 15, 20, 25, 30 Hz.

After microprocessing, the surface morphology was observed by Taylor Hobson profilometer/Talysurf PGI and Scanning Electron Microscope (SEM) JEOL/JSM-5600.

3. Results and Discussion

3.1. Influence of Laser Feedrate (Scanning Speed)

The initial surface with a surface roughness of 0.4 *μ*m was irradiated with laser pulse frequency (*f*) of 25 Hz, pulse energy of (*P*) 1 J, and pulse duration (*PD*) of 3 ms. The correlated results are shown in Figure **3**. Compared to Figure **3** with Figure **1**, and if the parameters are not set properly, the surface will be rather roughened than smoothened though most of the high plateaus are removed from the initial specimen surface.

It suggests that when the feed rate (scanning speed) is 300 mm/min, the achieved 3D morphology of the irradiated surface is the smoothest. It also shows that with the variation of laser feed rates, the irradiated surface changes correspondingly. During the period of between 100 mm/min and 300 mm/min, the irradiated surface becomes smoother. However, when the feed rate is higher than 300 mm/min, the quality of the irradiated surface will be coarser. Figures **3a** and **3b** depict the 3D morphology of the improved smoothness of processed surface with laser feedrate slower than 300 mm/min, and Figure **3d** shows the 3D morphology of unsmooth processed surface with laser feedrate higher than 300 mm/min.
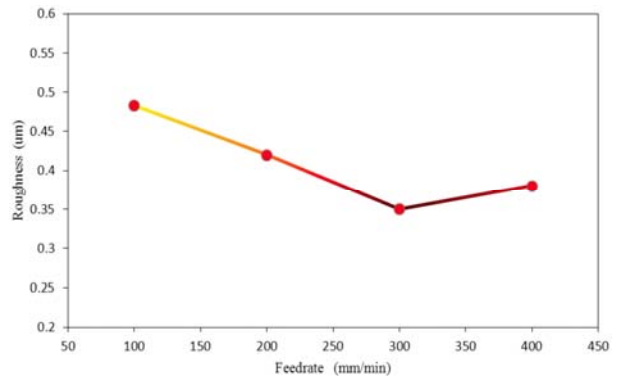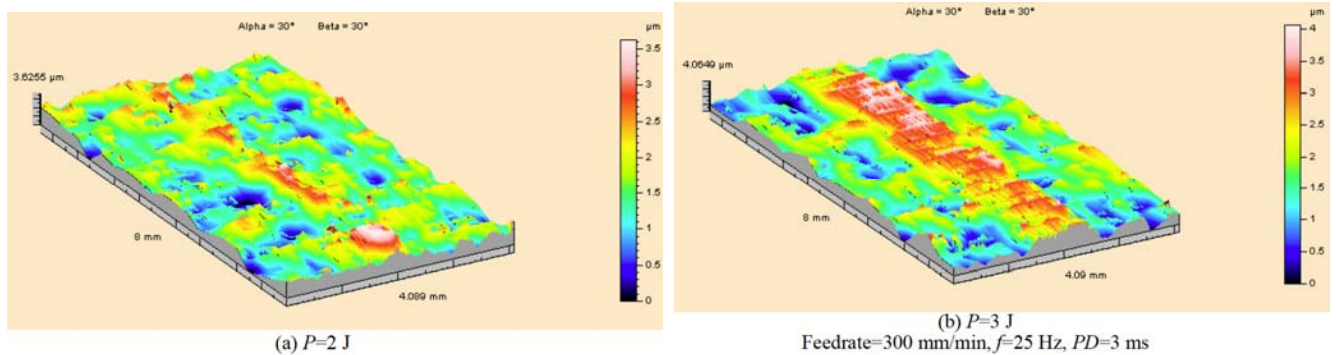

Figure 4: Relationship between surface roughness and feedrate.

The relationship between laser feedrate and the roughness of the processed surface is shown in Figure **4**. It indicates that when laser feedrate increases, the roughness of the processed surface will be decreased correspondingly. When the feedrate is at 400 mm/min, the irradiated roughness is increased to some level. Moreover, when the laser feedrate is up to 300 mm/min, the roughness of the processed surface is at its minimum. After that, with the laser feedrate increasing further, the roughness of the processed surface will be increased again. Moreover, the roughness of the processed surface is generally higher than the initial condition when the feedrate is below 300 mm/min. However, it decreases with the increase in the feedrate.

3.2. Influence of Laser Pulse Energy (*P*)

According to the study mentioned above, laser feedrate was taken as 300 mm/min in the subsequent tests as the optimal feedrate. The relationship between the roughness of the

Figure 5: Surface morphology of laser microprocessing at various laser pulse energies.

processed surface and laser pulse energy is shown in Figure **5**.

It is well known that if the laser pulse energy rises, the energy interaction between the workpiece and laser will be raised simultaneously when laser pulse energy is so high that the energy input into the workpiece will be obviously enhanced. As a result, the surface of the workpiece will melt, and the roughness of the processed surface will change seriously, significantly deteriorating the mechanical properties of the processed workpiece in subsequent practical applications.
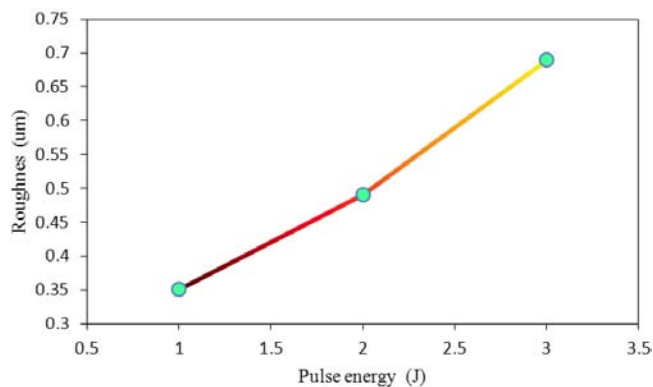
Figure 6: Relationship between surface roughness and pulse energy.

Figure **6** shows the relationship between the roughness of the processed surface and laser pulse energy. The results indicate that the roughness variation of the processed surface is correlated with laser pulse energy. When laser pulse energy (*P*) is 2 J, the roughness of the processed surface is 0.49 *µ*m with some protrusions distributed on the surface, as shown in Figure **5a**. With the increment of laser pulse energy, more protrusions are distributed on the processed surface. Consequently, the roughness of the processed surface will be up to 0.7 *µ*m. Meanwhile, the laser-affected zone is becoming wider and larger, as shown in Figure **5b**, which indicates if laser pulse energy is equal to or higher than 2 J, the results of the final micro-processed surface are generally not acceptable.

The correlated SEM results are shown in Figure **7**. It can be noted that Figure **7b** (the further magnified counterpart of

Figure **7a**) shows the sign of some micro-pits and round agglomerates loosely scattering over both troughs and crests on the surface. Those round agglomerates would be the nucleus for re-solidifying the melt and subsequent shrinkage led to some locations slightly sinking below their surrounding material. Such surface topography with a scattering of micro-pits and micro ball-like features (Figure **7b**) implies that there is some level of change in the properties of the AISI-O1 steel surface. This change is not really anticipated since it is initially expected, from Figure **7a**, that the properties of the original surface morphology at a pulse energy of 2 J would be the same as its as-received condition. At higher pulse energy (*i.e.*, 3 J), except those originally machining grooves ridges (Figure **7c**) that scattering on the irradiated surface with a shallower depth, more severe melting and re-solidification are observed. A large number of micro-holes and web-like cracks are distributed on the processed surface (Figures **7c** and **7d**). Such melting and re-solidification (Figure **7d**) drastically change the properties of the initial surface.

3.3. Influence of Laser Pulse Frequency (*f*)

Figure **8** shows the laser-irradiated surface scanned at various pulse frequencies. It indicates that the roughness of the irradiated surface decreases with the pulse frequency increasing. However, at a pulse frequency of 30 Hz, the roughness of the processed surface is distinctively higher again, resulting in a coarser finished surface. The corresponding roughness of the processed surface varied with laser pulse energy is shown in Figure **9**. The results illustrate when laser pulse frequency varies from 20 Hz to 25 Hz, the roughness of the processed surface is less than 0.4 *µ*m and the processed surface is smoother at the optimal level. However, the roughness of the processed surface will be increased obviously in case the laser pulse frequency increases higher, *e.g.*, 30 Hz. The correlated SEM results are shown in Figure **10**, which is coincident with the results shown in Figures **8** and **9**.

3.4. Influence of Laser Pulse Duration (*PD*)

Figure **11** shows the relationship between laser pulse duration and the roughness of the processed surface. The results illustrate that when the laser pulse duration is
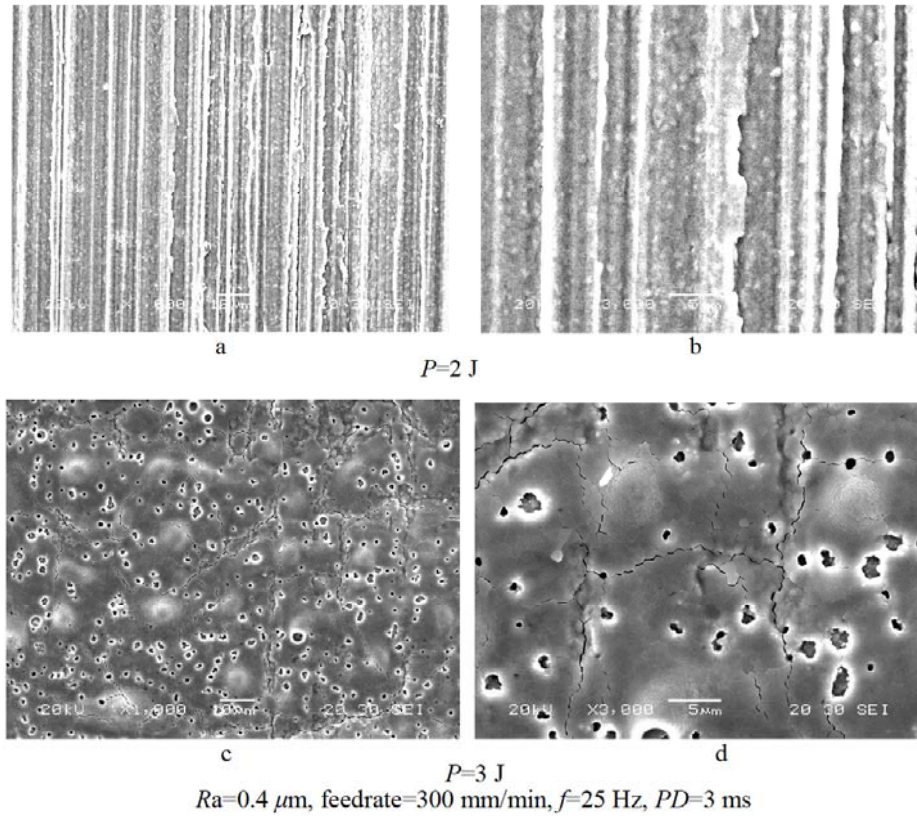
Figure 7: SEM results of laser micro-processed surface morphology at various pulse energies.
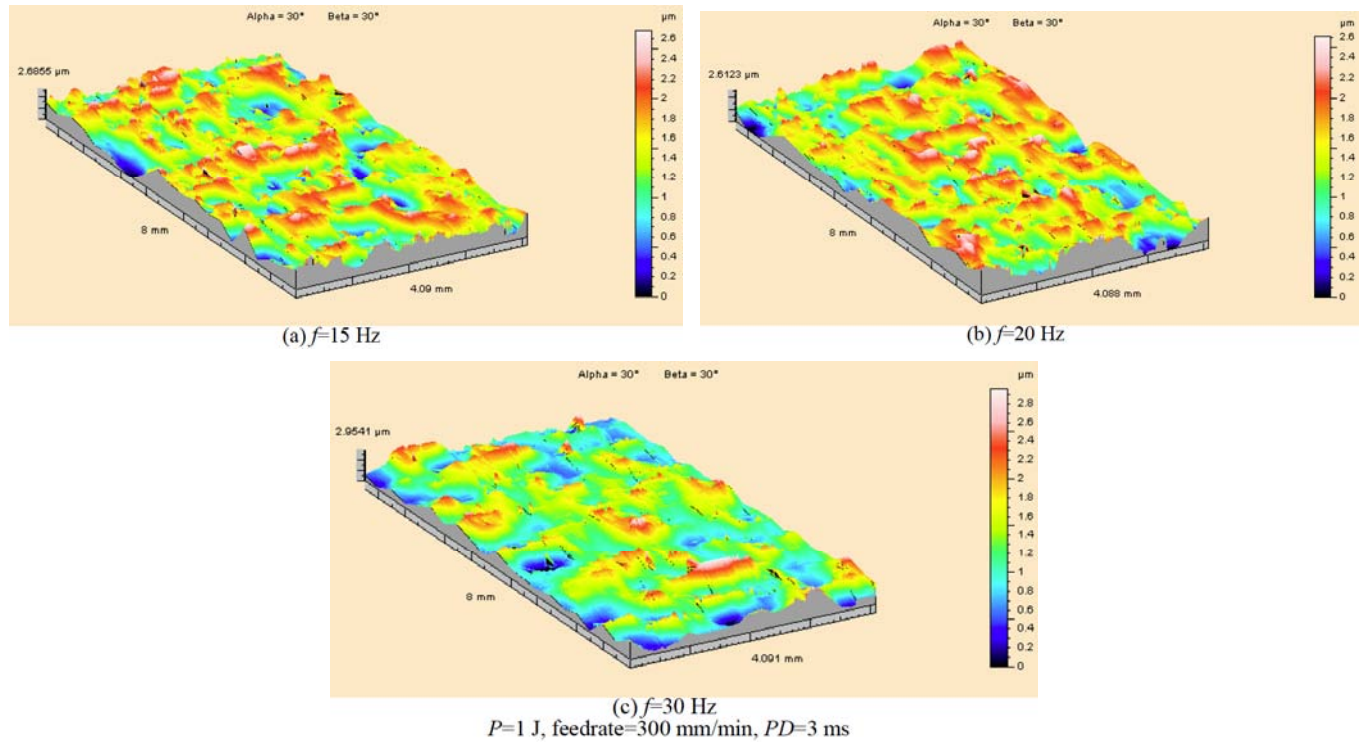

Figure 8: Surface morphology of laser microprocessing cat various pulse frequencies.
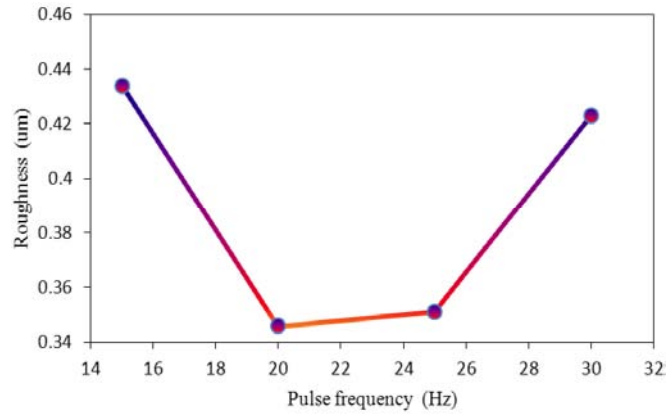
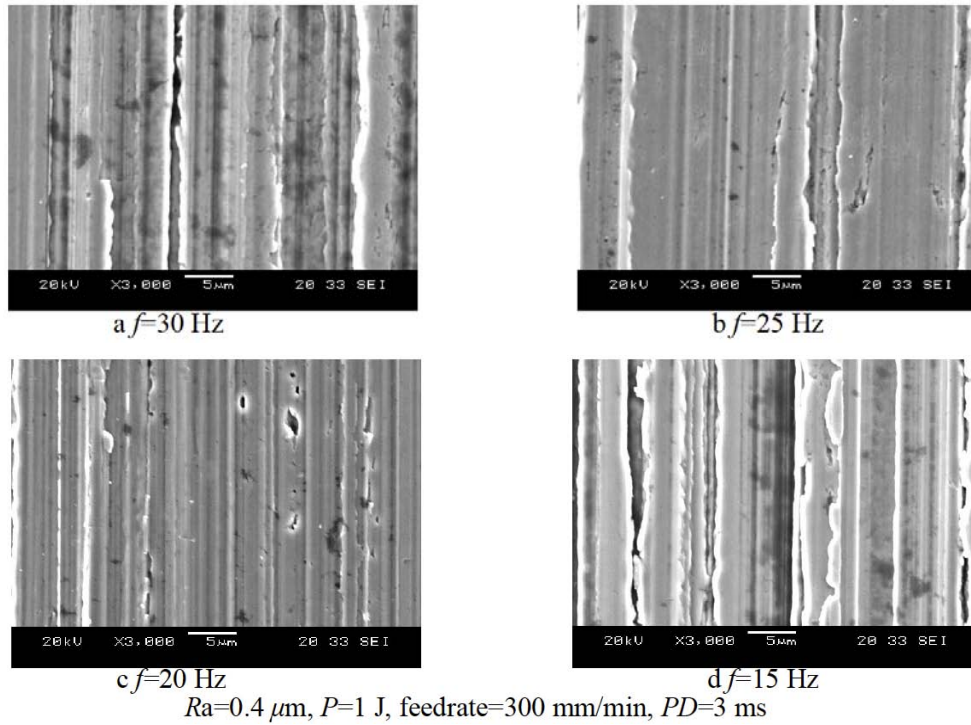**Figure 9:** Relationship between surface roughness and pulse frequencies.

a f=30 Hz

b f=25 Hz

c f=20 Hz

d f=15 Hz

Ra=0.4 μm, P=1 J, feedrate=300 mm/min, PD=3 ms

Figure 10: SEM results of laser micro-processed surface morphology at various pulse frequencies.
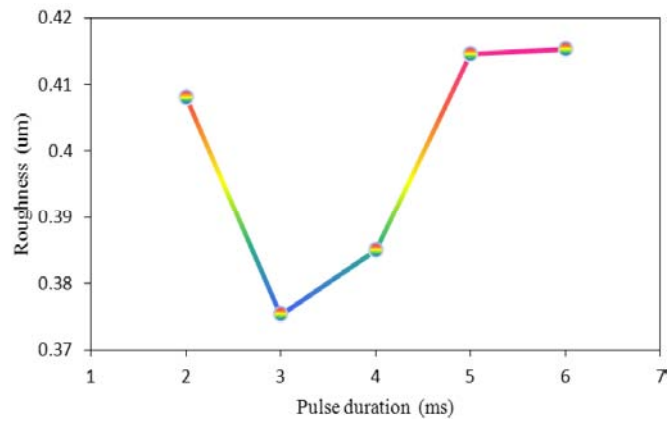
Figure 11: Relationship between surface roughness and pulse duration.

a *PD*=2 ms　　　　　b *PD*=3 ms　　　　　c *PD*=4 ms

d *PD*=5 ms　　　　　e *PD*=6 ms

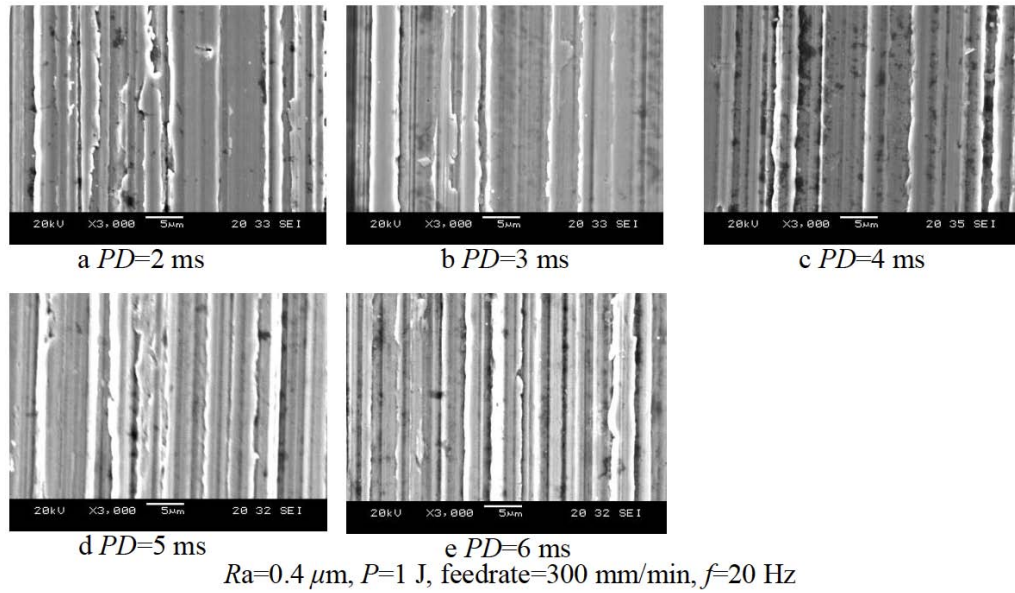*R*a=0.4 μm, *P*=1 J, feedrate=300 mm/min, *f*=20 Hz

Figure 12: SEM results of laser micro-processed surface morphology at various pulse durations.

decreased, the roughness of the processed surface will be decreased correspondingly. It also shows that the roughness of the processed surface is at its minimum when the laser pulse duration is 3 ms. With the decrement of laser pulse duration further (*e.g.*, 2 ms), the roughness of the processed surface will be increased remarkably. In addition, the roughness of the processed surface will be coarser when the laser pulse duration exceeds 4 ms. The relevant SEM results are shown in Figure **12**.

4. DISCUSSION

4.1. Influence of Feedrate and Pulse Frequency

As the irradiation path of a continuous scanning mode using a pulsed laser with pulse duration (*PD*) and frequency (*f*) is essentially consisting of a series of overlapping spots (Figure **13**), the basic condition to realize microprocessing by a pulsed laser is that two successive spots in a continuous scanning mode should be tangential to each other, *viz.*

$$0 < \delta \le D \tag{Eq. 1}$$

Where: *D* is the laser spot diameter, δ is the distance of one pulse (δ_1: the distance with the laser-on duration; δ_2: the distance with the laser-off duration.), and it is defined as:

$$\delta = \frac{Feedrate}{f} \tag{Eq. 2}$$

Substituting Eq. (2) into Eq. (1) subsequently gives:

$$0 < \frac{Feedrate}{f} \le D \tag{Eq. 3}$$

which can then be expressed as:
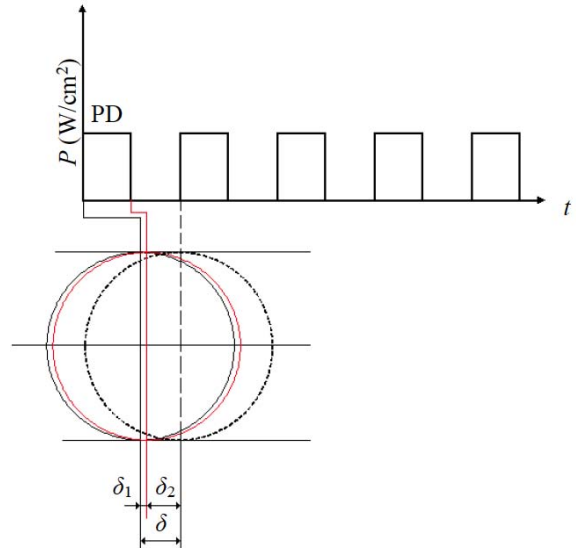
$$0 < Feedrate \le Df \tag{Eq. 4}$$

Figure 13: Schematic image of a laser pulse irradiated on the surface.

Figure **14** shows the relationship between δ and *f* (see Eq. (2)) at various feedrates and its corresponding percentage of overlapping of two successive laser pulses in the continuous scanning mode. It shows that the laser frequency increased: (i) with the decrease of δ (see the solid lines in Figure **14**); and (ii) simultaneously with an increase in the overlap percentage (see the dash lines in Figure **14**). When the feedrate is at 300 mm/min, the pulse frequency of 20~25 Hz leads to the δ is about 0.25~0.20 mm and the overlap percentage is about 60~68%.

Under the conditions of the experimental feedrates and pulse frequencies in this research, the distances of a single laser pulse (δ) are thus smaller than the laser spot diameter (*D*), which meets the constraint of Eq. (1) for the realization of laser microprocessing phenomenon. The mechanisms
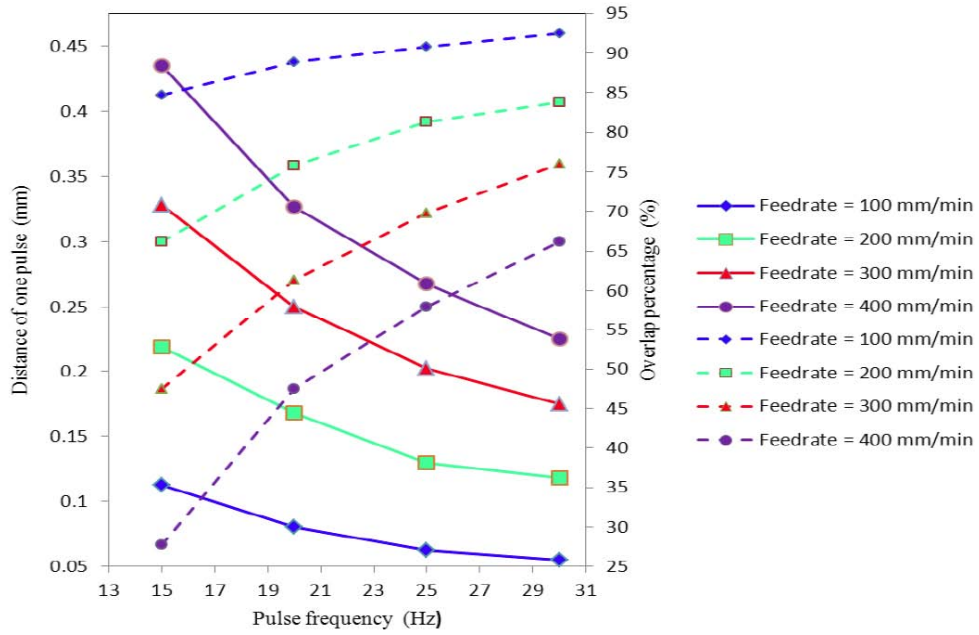
Figure 14: Relationship between δ and pulse frequency at various feed rates.
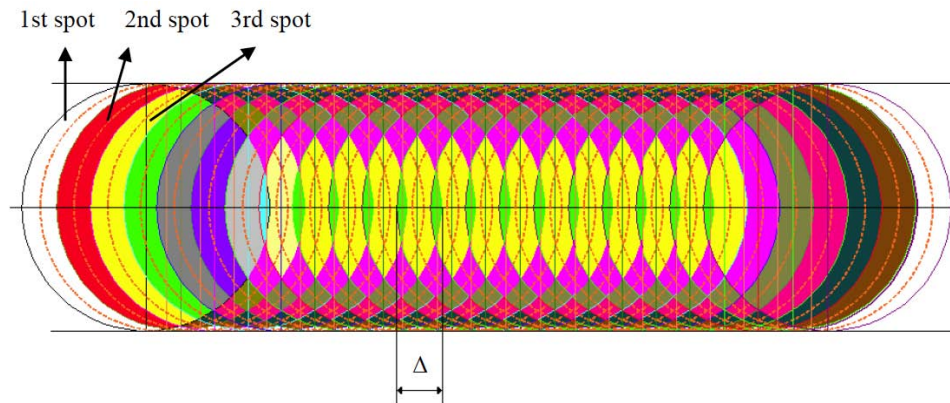

Figure 15: Schematic diagram of laser microprocessing.

involved in achieving the microprocessing effect at the operational parameters of pulse frequency f=20~25 Hz and feedrate= 300 mm/min are explored as follows.

In view of the overlapping geometry of the irradiation spot under continuous scanning mode, the laser microprocessing process is in a quasi-steady state (Figure **15**) when the moving distance of the spot within a single pulse is equal to or greater than the spot diameter. The solid lines with different colors in Figure **15** present the laser spot during the "on"-duration (δ_1 in Figure **13**) of a *PD*, while their individual counterpart dash lines respectively stand for the shifting of the laser spot during the "off"-duration (δ_2 in Figure **13**) of the *PD*. The areas filled with various colors in Figure **15** stand for the level of different overlapping (typically: the area in red color stands for the occurrence of only one overlap; the area in light yellow stands for the occurrence of two overlapping, *etc.*). Let Δ be the effective microprocessing size along the central line, and it can then be expressed as:

$$\Delta = D - \left\|\frac{D}{\delta}\right\| \times \delta + \delta \qquad \text{(Eq. 5)}$$

Figure **16** shows the behaviors of effective overlap percentage versus pulse frequency at the experimental feedrates. It shows that the relative overlap percentage for the feedrate = 300 mm/min is lower than that of other feedrates when the pulse frequency is at and beyond 20 Hz. When the pulse frequency is below 20 Hz, the effective overlap percentage is distinctly increased with the decrement in pulse frequency. Experimentally, the irradiated specimens with a smaller overlap percentage seem to give a better metallurgical aspect. This suggests that the surface can be microprocessing successfully according to various feedrates and pulse frequencies. When the effective overlap percentage inclines to null, the laser microprocessing will be of the ideal conditions as generated by single spot irradiation. Under such conditions, it gives:
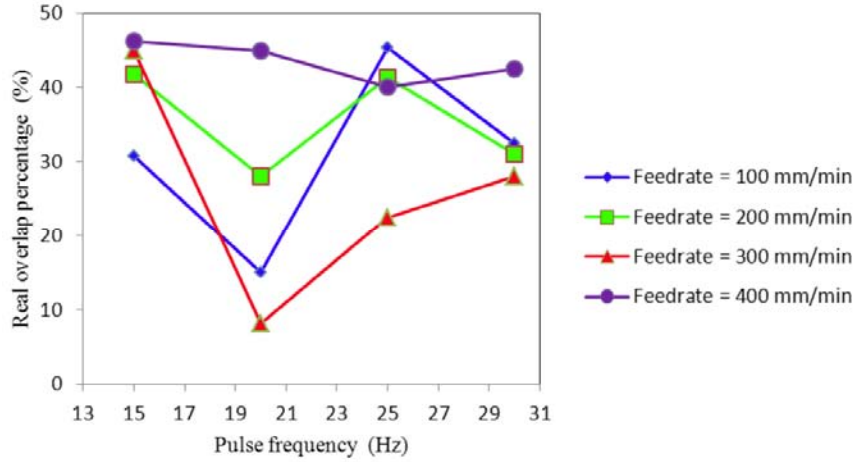
Figure 16: Effective overlapping percentage versus pulse frequency at various feed rates.

$$\left\| \frac{D}{\delta} \right\| = 0 \qquad \text{(Eq. 6)}$$

Subsequently, substituting Eq. (2) with Eq. (6) gives:

$$\left\| \frac{D \times f}{Feedrate} \right\| = 0 \qquad \text{(Eq. 7)}$$

Taking D=1.26 mm, Eq. (7) is therefore transformed into

$$126 \times f = 100 \times n \times Feedrate \ (f, n=1, 2, 3 \cdots) \quad \text{(Eq. 8)}$$

in which n stands for the number of macroscopical overlaps. When n is equal to 1, the two continuous laser spots are tangential to each other, implying both macroscopical overlap percentage and effective overlap percentage are equal to zero. At f is 20 Hz and feedrate is 300 mm/min, it can be deduced that the value of n is, therefore 5, which subsequently leads to an 80% (4/5) macroscopical overlap percentage and 20% (1/5) effective overlap percentage. When f is 20 Hz, the ideal feed rate is thus estimated as $\frac{126 \times 20}{5 \times 100} \times 60 = 302.4$ mm/min, which is very close to 300 mm/min. This is the reason why the morphology of the micro-processed surface is better when the laser is set at a pulse frequency of 20 Hz and feedrate of 300 mm/min.

4.2. Influence of Laser Pulse Energy and Pulse Duration (PD)

Figure **17** shows the model with a point source irradiating on a heavy substrate. The assumption of instantaneously releasing the laser energy on the surface of a substrate at time $t = 0$ leads to a temperature rise in the material (point P) as [21, 22]:

$$T - T_0 = \frac{Q}{\rho c (4\pi\alpha t)^{\frac{3}{2}}} \exp\left(\frac{-R^2}{4\alpha t}\right) \qquad \text{(Eq. 9)}$$

where ρ is the material density, C is specific heat, α is thermal diffusivity, *and* Q is the input energy. Let the initial temperature, at time t=0, of the generally thick plate be T_0,

and the point source of constant power q_0 moves in the x-direction at a constant speed (feedrate) v from position O.
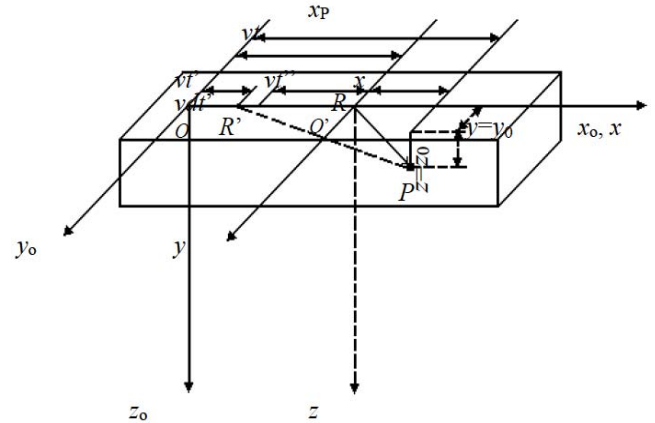

Figure 17: Moving point source on a semi-infinite substrate.

Within a very short interval of time t' $t' + dt'$, the amount of heat released at the surface is $dQ = q_o dt'$. By Eq. (9), it produces an infinitesimal temperature rise for the point P at time t as:

$$dT = \frac{2q_o dt'}{\rho c \left(4\pi\alpha (t - t')\right)^{\frac{3}{2}}} \exp\left(-\frac{\left(R'\right)^2}{4\alpha (t - t')}\right) \qquad \text{(Eq. 10)}$$

By defining $t'' = t - t'$, Eq. (10) is thus transformed into:

$$dT = \frac{-2q_o dt''}{\rho c \left(4\pi\alpha t''\right)^{\frac{3}{2}}} \exp\left(-\frac{\left(R'\right)^2}{4\alpha t''}\right) \qquad \text{(Eq. 11)}$$

Geometrically, Figure **17** allows $R' = \sqrt{\left(x_o - vt'\right)^2 + y_o{}^2 + z_o{}^2}$ being expressed. Subsequently, transforming the coordinate system from O to O': $y = y_o$, $z = z_o$, $x = x_o - vt$, and $x_o - vt' = x + vt - vt' = x + vt''$ allows the following expression to be obtained.

$$dT = \frac{-2q_o dt''}{\rho c (4\pi\alpha t'')^{\frac{3}{2}}} \exp\left(-\frac{\left((x+vt'')^2 + y^2 + z^2\right)}{4\alpha t''}\right)$$

$$= \frac{-2q_o dt''}{\rho c (4\pi\alpha t'')^{\frac{3}{2}}} \exp\left(-\frac{vx}{2\alpha} - \frac{R^2}{4\alpha t''} - \frac{v^2 t''}{4\alpha}\right) 9 \qquad \text{(Eq. 12)}$$

where: $R = \sqrt{x^2 + y^2 + z^2}$

When temperature distribution is quasi-steady state, Eq. (12) can be expressed as:

$$T - T_o = \frac{q_o}{2\pi\rho c\alpha R} \exp\left(-\frac{v}{2\alpha}(R+x)\right) \qquad \text{(Eq. 13)}$$

where: $q_0 = \eta(N(f,v)) \times \dfrac{P}{\dfrac{\pi D^2}{4} \times PD} = \eta(N(f,v)) \times \dfrac{4P}{\pi D^2 \times PD}$ in

which $\eta(N(f,v))$ is the coefficient of laser microprocessing input energy and is directly proportional to either the number of macroscopical overlaps or the pulse frequency and feedrate. Hence, Eq. (13) can be expressed as:

$$T - T_o = \frac{2 \times \eta(N(f,v)) \times P}{\pi^2 D^2 \rho c\alpha R \times PD} \exp\left(-\frac{v}{2\alpha}(R+x)\right) \qquad \text{(Eq. 14)}$$

Define $\xi = \dfrac{1}{2\pi\rho c\alpha}$, then Eq. (14) can be written as:

$$T - T_o = \frac{\xi \times \eta(N(f,v)) \times P}{\dfrac{\pi D^2}{4} \times PD \times R} \exp\left(-\frac{v}{2\alpha}(R+x)\right) \qquad \text{(Eq. 15)}$$

Equation 15 expresses the relationship between the laser microprocessing temperature and the processing parameters like: pulse energy, pulse duration, pulse frequency, and scanning speed (feedrate). The equation indicates that the increase in pulse energy and pulse frequency generally raises the microprocessing temperature. However, an increase in pulse duration and scanning speed (feedrate) accompanies a decrease in microprocessing temperature; whilst the increase in feedrate (scanning speed) leads to a decrease in the number of overlaps under the constant pulse frequency condition, implying that synchronously decrease in $\eta(N)$ and microprocessing temperature. Feedrate (scanning speed) generally has a more remarkable impact on the microprocessing temperature than the other parameters. At a particular feed rate, there tends to have a threshold of pulse energy, pulse duration, and pulse frequency for laser microprocessing successfully. Let's define:

$$q = \frac{P}{\dfrac{\pi D^2}{4} \times PD}, \qquad \text{(Eq. 16)}$$

Equation 15 can then be written as

$$T - T_o = \frac{\xi \times \eta(N(f,v)) \times q}{R} \exp\left(-\frac{v}{2\alpha}(R+x)\right) \qquad \text{(Eq. 17)}$$

Define:

Dimensionless temperature:

$$\omega_T = \frac{T - T_o}{T_r - T_o} \qquad \text{(Eq. 18)}$$

where T_r is the reference temperature.

Define:

Dimensionless operating parameter:

$$\kappa = \frac{\eta(N(f,v))qv}{4\pi\alpha^2 \rho c (T_r - T_o)} \qquad \text{(Eq. 19)}$$

Dimensionless x-coordinate:

$$\omega_x = \frac{vx}{2\alpha} \qquad \text{(Eq. 20)}$$

Dimensionless y-coordinate:

$$\omega_y = \frac{vy}{2\alpha} \qquad \text{(Eq. 21)}$$

Dimensionless z-coordinate:

$$\omega_z = \frac{vz}{2\alpha} \qquad \text{(Eq. 22)}$$

Dimensionless radius vector:

$$\omega_r = \frac{vR}{2\alpha} \qquad \text{(Eq. 23)}$$

Substituting these parameters into Eq. (17), then we have:

$$\omega_T = \frac{T - T_o}{T_r - T_o} = \kappa \frac{1}{\omega_r} \exp(-\omega_r - \omega_x) \qquad \text{(Eq. 24)}$$

or

$$\frac{\omega_T}{\kappa} = \frac{1}{\omega_r} \exp(-\omega_r - \omega_x) \qquad \text{(Eq. 25)}$$

Then the isothermal zone widths can be gotten just as fellows.

The maximum width of an isothermal enclosure is obtained by setting:

$$\frac{\partial \ln\left(\dfrac{\omega_T}{\kappa}\right)}{\partial \omega_r} = \frac{\partial \ln\left(\dfrac{\omega_T}{\kappa}\right)}{\partial \omega_x} \frac{\partial \omega_x}{\partial \omega_r} = 0 \qquad \text{(Eq. 26)}$$

where $\dfrac{\partial \omega_x}{\partial \omega_r} = \dfrac{\partial \omega_x}{\partial \sqrt{\omega_x + \omega_y + \omega_z}} = \dfrac{\omega_r}{\omega_x}$

Hence Eq. (26) will be transformed into:

$$\frac{\partial \ln\left(\dfrac{\omega_T}{\kappa}\right)}{\partial \omega_r} = \left(\left(-\frac{\omega_x}{\omega_r^2} - \frac{\omega_x}{\omega_r} - 1\right)\frac{\omega_r}{\omega_x}\right)_m = \left(-\frac{1}{\omega_r} - 1 - \frac{\omega_r}{\omega_x}\right)_m = 0 \text{ (Eq. 27)}$$

i.e.

$$\omega_{xm} = -\frac{\omega_{rm}{}^2}{\omega_{rm}+1} \qquad \text{(Eq. 28)}$$

Substituting ω_{xm} into Eq. (25), then we have:

$$\frac{\omega_{T_m}}{\kappa} = \frac{1}{\omega_{rm}}\exp(-\omega_{rm}-\omega_{xm}) = \frac{1}{\omega_{rm}}\exp\left(-\frac{\omega_{rm}}{\omega_{rm}+1}\right) \quad \text{(Eq. 29)}$$

Equation (25) shows the relationship between the laser microprocessing temperature and the processing parameters, such as pulse energy (P), pulse duration (PD), pulse frequency (f), feedrate, *etc*. It can be seen that with the pulse energy (P) and pulse frequency (f) increasing, the processing temperature will be higher. However, with the pulse duration (PD) and feedrate increasing, the processing temperature will be decreased. Furthermore, when the feed rate is increased, $\eta\big(N(f,v)\big)$ it will be decreased synchronously. Therefore, the processing temperature will be decreased seriously. Furthermore, according to Eq. (23) and Eq. (29), it indicates that the feedrate has a more remarkable impact on the processing temperature of the given points. Therefore, there is a certain heat-input threshold with a certain pulse feedrate, pulse energy (P), pulse duration (PD), and pulse frequency (f) for laser microprocessing.

5. CONCLUSIONS

1. Pulsed Nd: YAG laser can be taken successfully for microprocessing AISI-O1 cold work steel. The optimum laser microprocessing parameters achieved by experiments are P=1 J, feedrate=300-400 mm/min, PD=3-4 ms, f=20~25 Hz.

2. According to the onset of laser processing temperature, $T - T_o = \dfrac{\xi \times \eta\big(N(f,v)\big) \times q}{R}\exp\left(-\dfrac{v}{2\alpha}(R+x)\right)$ the morphology of the laser micro-processed surface can be controlled with the relevant processing parameters, which is attractive and beneficial to practical applications in the microprocessing world.

3.The maximum width of an isothermal enclosure of laser microprocessing is $\dfrac{\omega_{T_m}}{\kappa} = \dfrac{1}{\omega_{rm}}\exp\left(-\dfrac{\omega_{rm}}{\omega_{rm}+1}\right)$, where the feed rate has a more remarkable impact on the processing temperature of the given points.

REFERENCES

[1] Steen WM. Laser Material Processing, 3rd ed. London: Springer-Verlag; 2003.
https://doi.org/10.1007/978-1-4471-3752-8

[2] De Zanet A, Casalegno V, Salvo M. Laser surface texturing of ceramics and ceramic composite materials - A review. Ceramics International 2021; 47(6): 7307-7320.
https://doi.org/10.1016/j.ceramint.2020.11.146

[3] Sahu AK, Malhotra J, Jha S. Laser-based hybrid micromachining processes: A review. Optics & Laser Technology 2022; 146: 107554.
https://doi.org/10.1016/j.optlastec.2021.107554

[4] Ali B, Litvinyuk IV, Rybachuk M. Femtosecond laser micromachining of diamond: Current research status, applications, and challenges. Carbon 2021; 179: 209-226.
https://doi.org/10.1016/j.carbon.2021.04.025

[5] Lugomer S. Laser Technology-Laser Driven Processes. Englewood Cliffs, N.J.: Prentice Hall; 1990: 419-439.

[6] Duley WW. Laser Processing and Analysis of Materials. New York and London: Plenum Press; 1983.
https://doi.org/10.1007/978-1-4757-0193-7

[7] Jagannadham K, Watkins TR, Lance MJ, Riester L, Lemaster RL. Laser physical vapor deposition of boron carbide films to enhance cutting tool performance. Surface and Coatings Technology 2009; 203(20-21): 3151-3156.
https://doi.org/10.1016/j.surfcoat.2009.03.049

[8] Machado AR, da Silva LRR, de Souza FCR, Davis R, Pereira LC, Sales WF, de Rossi W, Ezugwu EO. State of the art of tool texturing in machining. Journal of Materials Processing Technology 2021; 293: 117096.
https://doi.org/10.1016/j.jmatprotec.2021.117096

[9] Siddiqui AA, Dubey AK. Recent trends in laser cladding and surface alloying. Optics & Laser Technology 2021; 134; 106619.
https://doi.org/10.1016/j.optlastec.2020.106619

[10] Rosenkranz A, Costa HL, Baykara MZ, Martini A. Synergetic effects of surface texturing and solid lubricants to tailor friction and wear – A review. Tribology International 2021; 155: 106792.
https://doi.org/10.1016/j.triboint.2020.106792

[11] Dong J, Pacella M, Liu Y, Zhao L. Surface engineering and the application of laser-based processes to stents - A review of the latest development. Bioactive Materials 2022; 10: 159-184.
https://doi.org/10.1016/j.bioactmat.2021.08.023

[12] Krimpenis AA, Noeas GD. Application of hybrid manufacturing processes in microfabrication. Journal of Manufacturing Processes 2022; 80: 328-346.
https://doi.org/10.1016/j.jmapro.2022.06.009

[13] Mao B, Siddaiah A, Liao YL, Menezes PL. Laser surface texturing and related techniques for enhancing tribological performance of engineering materials: A review. Journal of Manufacturing Processes 2020; 53: 153-173.
https://doi.org/10.1016/j.jmapro.2020.02.009

[14] Vishnoi M, Kumar P, Murtaza Q. Surface texturing techniques to enhance tribological performance: A review. Surfaces and Interfaces 2021; 27: 101463.
https://doi.org/10.1016/j.surfin.2021.101463

[15] Ijaola AO, Bamidele EA, Akisin CJ, Bello IT, Oyatobo AT, Abdulkareem A, Farayibi PK, Asmatulu E. Wettability Transition for Laser Textured Surfaces: A Comprehensive Review. Surfaces and Interfaces 2020; 21: 100802.
https://doi.org/10.1016/j.surfin.2020.100802

[16] Stratakis E, Bonse J, Heitz J, Siegel J, Tsibidis GD, Skoulas E, Papadopoulos A, Mimidis A, Joel AC, Comanns P, Krüger J, Florian C, Fuentes-Edfuf Y, Solis J, Baumgartner W. Laser engineering of biomimetic surfaces. Materials Science and Engineering: R: Reports 2020; 141: 100562.
https://doi.org/10.1016/j.mser.2020.100562

[17] Sohn IB, Choi HK, Noh YC, Kim JY, Ahsan MS. Laser assisted fabrication of micro-lens array and characterization of their beam shaping property. Applied Surface Science 2019; 15: 375-385.
https://doi.org/10.1016/j.apsusc.2019.02.083

[18] Gautam GD, Pandey AK. Pulsed Nd:YAG laser beam drilling: A review. Optics & Laser Technology 2018; 100: 183-215.
https://doi.org/10.1016/j.optlastec.2017.09.054

[19] Ijaola AO, Bamidele EA, Akisin CJ, Bello IT, Oyatobo AT, Abdulkareem A, Farayibi PK, Asmatulu E. Wettability transition for laser textured surfaces: A comprehensive review. Surfaces and Interfaces 2020; 21; 100802.
https://doi.org/10.1016/j.surfin.2020.100802

[20] Shrivastava A, Mukherjee S, Chakraborty SS. Addressing the challenges in remanufacturing by laser-based material deposition techniques. Optics & Laser Technology 2021; 144: 107404.
https://doi.org/10.1016/j.optlastec.2021.107404

[21] Janna WS. Engineering Heat Transfer. Boston: PWS Engineering; 1986.

[22] Jastrzebski ZD. The Nature and Properties of Engineering Materials, 3rd ed., New York: John Wiley & Sons Inc.; 1987.